All-quantum simulations: H_3O^+ and $H_5O_2^+$

H.-P. Cheng, R.N. Barnett, Uzi Landman

School of Physics, Georgia Institute of Technology, Atlanta, GA 30332, USA

Received 29 October 1994; in final form 6 March 1995

Abstract

Electronic structure calculations using the local density functional method with non-local norm-conserving pseudopotentials, ab initio molecular dynamics simulations, and a novel method of all-quantum simulations, combining a quantum path-integral description of the nuclear degrees of freedom with concurrent electronic structure calculations of the Born–Oppenheimer potential energy surface, were employed in investigations of the structure and dynamics of protonated water clusters. Using electronic structure, structural optimization and all-quantum simulations, structures and energetics of H_3O^+, $(H_2O)_2H^+$, as well as NH_4^+, $(NH_3)_2H^+$, and the mixed $(NH_3)(H_2O)H^+$ cluster, are described and analyzed. The quantum nature of the hydrogens in the protonated water clusters, as well as a measure of the tunneling enhancement of the inversion isomerization in H_3O^+ at 150 K, are demonstrated and discussed.

1. Introduction

The most commonly used form of molecular dynamics (MD) simulations (see the collection of articles in Ref. [1]) involves numerical integration of the classical equations of motion of many-particle systems, with prescribed model inter-particle interaction potentials. Such classical and quantum-classical (see the review in Ref. [2]) simulations, while useful, are restricted by the inherent limitations of the interaction potentials, particularly under conditions which are outside the range of validity of the data-base used for parameterization or fitting of the potentials, and in circumstances involving electronic rearrangements. The introduction of 'ab initio' MD schemes where the classical dynamics of the ions evolves on the concurrently [3,4] (see also the reviews in Refs. [5,6]), quantum-mechanically calculated ground-state Born–Oppenheimer (BO) potential energy surface, alleviate certain of the aforementioned limitations.

In certain cases, as in systems containing light nuclei (particularly protons), considerations of the quantum mechanical nature of the nuclear degrees of freedom are important. To this end, simulation methods based on the path-integral (PI) formulation of quantum statistical mechanics [7] have been employed (see reviews in Refs. [8–12]) using model interaction potentials.

In this Letter we present an all-quantum molecular dynamics simulation method (AQMD), unifying the methodology of the BO local-density-functional MD (BO-LDA-MD) method [4] with the quantum PI description of the nuclear degrees of freedom. The new method offers new ways for investigating physical and chemical issues in molecular and condensed matter systems, particularly in systems involving light species, such as proton transfer processes, hydrogen bonding, tunneling, molecular liquids, ice, compressed hydrogen, quantum liquids, and clusters. Following a brief description of the new theoretical simulation method in Section 2, we give in Section 3 results pertaining to the energetics and structures of

protonated water and ammonia clusters. In Section 4 we apply the AQMD method to studies of the hydronium ion (H_3O^+) and the protonated water dimer $(H_2O)_2H^+$. We summarize our results in Section 5.

2. Method

The all-quantum simulation method combines the BO-LDA-MD method with the PI one. We give here a brief description (for details see Ref. [4]), followed by presentation of the new AQMD method.

2.1. The Born–Oppenheimer local-density-functional molecular dynamics (BO-LDA-MD) method

In simulations of the classical dynamics of ions on the ground-state BO electronic potential-energy surface, the dynamical evolution is generated via integration of the Newtonian equations of motion,

$$\nabla_I \ddot{r}_I = -\nabla_{r_I} E_{el}(\{r\}) - \nabla_{r_I} \sum_{I>J} \frac{Z_I Z_J}{|r_I - r_J|}, \qquad (1)$$

where r_I denotes the vector position of the Ith ion of charge Z_I, the second term on the right is the force on the ion due to the interionic Coulomb repulsion, and the first term is the force on the Ith ion due to its interaction with the ground state electronic density ($\{r\}$ denotes collectively the coordinates of all the ions in the system). Evaluation of the electronic force, via the Hellman–Feynman theorem [13], requires an efficient and accurate method for calculating the electronic energy E_{elec} for any ionic configuration, $\{r_I\}$.

In our calculations

$$E_{elec} = T_e + E_{eI} + E_{ee}, \qquad (2)$$

where T_e is the kinetic energy of the electrons, E_{eI} is the electron–ion interaction energy and E_{ee} is the electron–electron interaction energy, is evaluated after each classical molecular dynamics integration step (i.e. solution of Eq. (1) for the ionic coordinates), with the use of the local-density-functional (LDA), or the local-spin-density functional (LSD), method, and employing a plane-wave basis and nonlocal norm-conserving pseudopotentials [14]. We remark that in the simulations presented below we

used the local exchange–correlation (xc) functional [15], while in our optimization of the structures of the clusters we used generalized gradient corrections (GGC) where the exchange [16] and correlation [17] gradient corrections (xcg) are included in a self-consistent manner. We emphasize that while in our dual-space method we use plane-wave basis sets for finite systems, we do not employ a supercell procedure, i.e. there are no periodically repeated images of the system [4]. This has the advantage that it enables us to treat accurately finite systems which are charged or have large multipole moments as well as fragmentation and reaction processes in molecular and cluster systems.

Since in our method the electronic energy and forces on the nuclei are calculated during a dynamical simulation for each successive nuclear configuration, we are assured to remain on the ground-state BO surface throughout the evolution of the system, thus allowing a relatively large time step, Δt, in the integration of the classical nuclear equations of motion (determined by the highest characteristic vibrational frequencies in the system; thus, in simulations of water systems we used $\Delta t = 0.8$ fs, with a Gear fifth-order predictor–corrector algorithm, conserving energy to $\approx 10^{-4}\%$ of the total energy).

2.2. All-quantum simulations: the AQMD method

In all the above-mentioned simulations the nuclei were restricted to behave classically. For systems containing light nuclei, where considerations of the quantum mechanical nature of the nuclear degrees of freedom are of importance, simulation methods based on the path-integral (PI) formulation of quantum statistical mechanics [7] have been developed [8–12].

According to the Feynman path-integral formulation of quantum statistical mechanics, the partition function

$$Z = \text{Tr}(e^{-\beta H}) \qquad (3)$$

(where $\beta = 1/k_B T$, and Tr denotes a trace) for a system of N interacting distinguishable particles with the Hamiltonian H given by

$$H = \sum_{i=1}^{N} \frac{-\hbar^2}{2m_i} \nabla_i^2 + V(r_1, r_2, \ldots, r_N), \qquad (4)$$

may be written as

$$Z = \lim_{P \to \infty} Z_P, \qquad (5)$$

where

$$Z_P = \int \left(\prod_{i=1}^{N} \prod_{\alpha=1}^{P} dr_i^{(\alpha)} \right) \prod_{i=1}^{N} \prod_{\alpha=1}^{P} E\left(r_i^{(\alpha)}, r_i^{(\alpha+1)}; \epsilon \right)$$

$$\times \exp\left(-\epsilon \sum_{\alpha=1}^{P} V\left(r_1^{(\alpha)}, \ldots, r_N^{(\alpha)} \right) \right). \qquad (6)$$

In Eq. (6) $\epsilon = \beta/P$, and

$$E\left(r_i^{(\alpha)}, r_i^{(\alpha+1)}; \epsilon \right)$$

$$= \left(\frac{P}{2\pi\lambda_i^2} \right)^{3/2} \exp\left(-\frac{P}{2\lambda_i^2} \left(r_i^{(\alpha)} - r_i^{(\alpha+1)} \right)^2 \right),$$

$$(7)$$

where the characteristic length $\lambda_i^2 = \hbar^2\beta/m_i$ is the thermal wavelength (or uncertainty spreading) of a free particle of mass m_i.

In this description each quantum particle maps onto an isomorphic 'ring polymer' (or cyclic 'necklace'), consisting of P pseudo-particles (or 'beads'; in general we could have assigned to each particle a different number of beads), held together by harmonic springs. We note that in the limit of large mass m_i each of the factors $E(r_i^{(\alpha)}, r_i^{(\alpha+1)})$ approaches $\delta(r_i^{(\alpha)} - r_i^{(\alpha+1)})$ and the corresponding necklace 'collapses' to a single point in space, r_i. This is the classical limit which can similarly be achieved for high temperature, i.e. small β, with necklaces corresponding to particles of larger mass collapsing first. Since $\lambda^2 = 48 \text{ Å}^2$ amu K/Tm, we note that for hydrogen $\lambda^2(\text{H}, T) = 48 \text{ Å}^2$ K/T while for oxygen $\lambda^2(\text{O}; T) = 3 \text{ Å}^2$ K/T. Consequently, in a system consisting of oxygens and hydrogens, the oxygens may be assumed classical (i.e. single-bead necklaces, although as we will see below this does not bring a significant saving in computational time).

Specializing to a system consisting of N_H hydrogen atoms (protons) and N_O oxygens, Eq. (6) can be rewritten as

$$Z_P = \left(\frac{P}{2\pi\lambda_H^2} \right)^{3N_H P/2} \left(\frac{1}{2\pi\lambda_O^2} \right)^{3N_O/2}$$

$$\times \int \prod_{i=1}^{N_H} \prod_{\alpha=1}^{P} dr_i^{(\alpha)} \prod_{j=1}^{N_O} dr_j \exp(-\beta V_P),$$

$$(8)$$

with

$$V_P = \frac{P m_H}{2(\hbar\beta)^2} \sum_{\alpha=1}^{P} \sum_{i=1}^{N_H} \left(r_i^{(\alpha)} - r_i^{(\alpha+1)} \right)^2$$

$$+ \frac{1}{P} \sum_{\alpha=1}^{P} V\left(r_1^{(\alpha)}, \ldots, r_{N_H}^{(\alpha)}; r_1, \ldots, r_{N_O} \right), \qquad (9)$$

where m_H is the proton mass, and r_j, $1 \leq j \leq N_O$, are the positions of the oxygen atoms (taken as classical particles).

The 'classical form' of the expression for the partition function in Eq. (8) is evident. However we iterate that in the limit of $P \to \infty$ it yields (rigorously) the value for the quantum partition function.

The quantum expectation value for any quantity $A(r)$, where r denotes collectively the coordinates of all particles in the 'real' physical system under consideration (hydrogens and oxygens in our case) is given in terms of averages over the canonical ensemble of a classical (isomorphic) system with a potential V_P (Eq. (9)),

$$\langle A \rangle = \lim_{P \to \infty} A_P$$

$$= \lim_{P \to \infty} \left[\frac{1}{Z_P} \int \left(\prod_{i=1}^{N_H} \prod_{\alpha=1}^{P} dr_i^{(\alpha)} \right) \right.$$

$$\times \prod_{j=1}^{N_O} dr_j \, A\left(r_1^{(\alpha)}, \ldots, r_{N_H}^{(\alpha)}; r_1, \ldots, r_{N_O} \right)$$

$$\left. \times \exp(-\beta V_P) \right]. \qquad (10)$$

The Boltzmann-weighted canonical averages in Eq. (10) may be evaluated via a Monte Carlo sampling of the configurational space of the isomorphic system, or (as in our simulations) through averaging over the phase-space trajectories generated in a MD simulation [18] via integration of the equations of motion obtained from the Hamiltonian for the isomorphic system,

$$H_P = \frac{1}{2} \sum_{i=1}^{N_H} \sum_{\alpha=1}^{P} m_H^* \left(\dot{r}_i^{(\alpha)} \right)^2 + \frac{1}{2} \sum_{j=1}^{N_O} m_O^* \left(\dot{r}_j \right)^2 + V_P,$$

$$(11)$$

where m_H^* and m_O^* are auxiliary (fictitious) masses of the pseudo-particles (beads), chosen such as to

enhance proper sampling of the phase-space of the isomorphic system.

The potential V in Eq. (9) is general. All PI simulations to date employed for V prescribed model interaction potentials, and have been applied with significant success to various systems [7–11,19–23]. However, these simulations share similar limitations, pertaining to the interaction potentials employed, as those mentioned above in the context of classical simulations. On the other hand, in our new *all-quantum* MD (AQMD) method the quantum nature of the nuclei is included (via the path-integral formulation) and the energetics (of the isomorphic system) on the self-consistent BO electronic potential energy surface is concurrently evaluated (via LDA or LSD). We remark in this context that while the nuclei are restricted to sample the (evolving) BO ground state electronic potential energy surface, they are free to thermally populate (with canonical ensemble statistical weights) excited (vibrational-like) states of the nuclear degrees of freedom.

Finally, we note from Eq. (9) that while the harmonic term (first term on the right-hand side) couples consequitive beads (α and $\alpha + 1$) of particle i, the interaction potential $V(r_1^{(\alpha)}, \ldots, r_{N_H}^{(\alpha)};$ $r_1, \ldots, r_{N_O})$ involves only beads with the same index α on different necklaces (i.e. corresponding to different particles). Thus in performing an ab initio BO-LSD-MD simulation for the isomorphic system, one needs to evaluate, at each integration step of the (Newtonian) equations of motion for the beads (derived from the Hamiltonian in Eq. (11)), the Born–Oppenheimer ground-state energies for P sets of coordinates; $(r_1^{(1)}, \ldots, r_{N_H}^{(1)}; r_1, \ldots, r_{N_O}), \ldots, (r_1^{(P)}, \ldots, r_{N_H}^{(P)}; r_1, \ldots, r_{N_O})$. Consequently, in such all-quantum simulations, where both the electrons and nuclei are treated quantum mechanically, the computational effort is P-fold multiplied in comparison to a simulation where the nuclei are treated classically (since the dominant portion of time in the simulation is spent in solving the electronic structure for given positions of the hydrogen beads (and oxygen nuclei). We additionally remark that the structure of the equations allows for significant gains in computa-

Table 1
Energetics and structural information of protonated clusters $A_n H^+$, $n = 1, 2$, for $A = H_2O$, NH_3 and $(NH_3)(H_2O)$

A	n		Δ_1	Δ_2	d_{BH^+}	d_{BH}	$\angle(HBH)$	$\angle(BH^+B)$
H_2O	1	LDA	7.361		0.984	–	114.2	
		GGC	7.519					
		exp.	7.229 [a]					
NH_3	1	LDA	9.065		1.019	–	109.47	
		GGC	9.30					
		exp.	8.871 [b]					
H_2O	2	LDA	8.90	1.934	1.197	0.964	110.4	174.5
		GGC	8.955	1.549				
		exp.		(1.370 [a], 1.431 [c], 1.561 [c])				
NH_3	2	GGC	10.452	1.233	1.307	1.014	107.5	180
		exp.		(1.075 [c], 1.17 [c], 1.10 [c])				
$(NH_3)(H_2O)$	1	GGC	9.936	0.877 [d]	1.561 [e]	0.961 [c]	107.2 [e]	177.9 [f]
				2.646 [g]	1.07 [h]	1.016 [h]	108.7 [h]	
		exp.		0.863 [c,d]				
				2.37 [c,g]				

The binding energy of H^+ to A_n (i.e. the proton affinity of A_n) is given by $\Delta_1 = E[A_n] - E[A_n H^+]$, and the solvation energy of AH^+ is given by $\Delta_2 = E[A_{n-1}H^+] + E[A] - E[A_n H^+]$. In the case of $(NH_3)(H_2O)H^+$ results for Δ_2 are given for $(NH_3)(H_2O)H^+ \rightarrow NH_4^+ + H_2O$, and $(NH_3)(H_2O)H^+ \rightarrow H_3O^+ + NH_3$. Energies are given for LDA calculations and for LDA calculations including exchange–correlation gradient corrections self-consistently (GCC), with plane-wave energy cutoff $E_c = 96$ Ry. The structural results correspond to GGC calculations with $E_c = 96$ Ry. The distances (d_{BH^+}, d_{BH}) and angles ($\angle(HBH)$, $\angle(BH^+B)$) are given for the clusters, with B corresponding to the O or N nuclei, respectively. Energies in eV, distances in Å, and angles in deg.
[a] Ref. [34].　[b] Ref. [31].　[c] For a compilation of data and references, see Ref. [35].
[d] $(NH_3)(H_2O)H^+ \rightarrow NH_4^+ + H_2O$.　[e] $B = O$.　[f] $\angle(OH^+N)$.　[g] $(NH_3)(H_2O)H^+ \rightarrow NH_3 + H_3O^+$.　[h] $B = N$.

tional efficiency via the use of parallel computational architectures.

In our simulations of protonated water and ammonia clusters we have employed norm-conserving non-local pseudo-potentials [14] for the oxygen and nitrogen atoms (s and p components, with s non-locality) and a local pseudo-potential for the hydrogens. In structural optimization plane-wave kinetic energy cutoffs, E_c, of 96 and 158 Ry were used. Both LDA calculations and generalized-gradient correction (GGC) calculations were performed. In the BO-LDA-MD and AQMD simulations for H_3O^+ and $(H_2O)_2H^+$ at 150 K, the BO potential energy surfaces were calculated via LDA with $E_c = 96$ Ry. In the path-integral MD the number of pseudo-particles $P = 8$, and an integration time-step of $\Delta t = 0.8$ fs was used. Statistical averages were obtained from simulations of up to $1.2 \times 10^4 \, \Delta t$.

3. Proton solvation in small clusters: energetics and structures

Protonated water clusters (the hydronium ion H_3O^+, and the hydrated hydronium $H_3O^+ \cdot nH_2O$, or $(H_2O)_nH^+$) are systems of importance in a number of areas of chemical and physical research, and have been the subject of several experimental and theoretical investigations (see the reviews in Ref. [24]) [25–33]. While in this study we focus on small protonated water clusters (H_3O^+ and $H_5O_2^+$), we compare first their energetics and structure to that of NH_4^+, and to $N_2H_7^+$ and the mixed $(NH_3)(H_2O)H^+$ cluster [1] (see Table 1 and Fig. 1).

Inspection of the energetics data displayed in Table 1 reveals several trends (based on GGC results). First, from comparison of the affinities (given by Δ_1 in Table 1) we conclude that:

(i) The calculated proton affinity of the ammonia
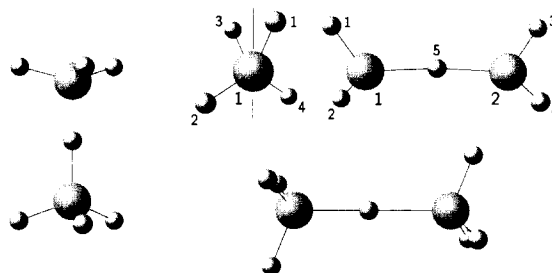
Fig. 1. Left: optimized structures (at the GGC level, with a plane-wave cutoff energy of 96 Ry) for H_3O^+ (C_{3v} symmetry) and NH_4^+ (tetrahedral); see Table 1. Small spheres correspond to hydrogens and large spheres to an oxygen or a nitrogen. For H_3O^+ the distance of the oxygen from the plane of hydrogens $h_O = 0.244$ Å and the angle between h_O and the OH bond $\theta = 75.8°$. For comparison, the calculated distances in H_2O and NH_3 are $d_{OH} = 0.964$ Å and $d_{NH} = 1.01$ Å, respectively, and $\angle(HOH) = 104.7°$ and $\angle(HNH) = 107.2°$. Right: optimized structures for $(H_2O)_2H^+$ (C_2 symmetry) and $(NH_3)_2H^+$, calculated via LDA-GGC with $E_c = 96$ Ry; see Table 1. For the $(H_2O)_2H^+$ cluster $d_{OO} = 2.39$ Å, $\angle(H_1OH^+) = 121.1°$, and $\angle(H_2OH^+) = 119.7°$ (the hydrogen atoms H_1 and H_2 are denoted in the figure and the inter-molecular proton is denoted as H_5). Calculations for $(H_2O)_2H^+$ using LDA-GGC, with $E_c = 158$ Ry yielded essentially the same structure with $d_{OH} = 0.973$ Å. Shown also is a view along the O_1O_2 axis, the angles δ_1, δ_2 between the projections of the O_1H_1 and O_1H_2 bonds on a plane normal to the O_1O_2 axis and the vertical line indicated in the figure, are 22.4° and 56.3°, respectively ($\delta_1 = 22.8°$ and $\delta_2 = 56.3°$ for $E_c = 158$ Ry). For the $(NH_3)_2H^+$ molecular ion the two proton-bonded NH_3 molecules are rotated by 60° with respect to each other about the NN axis.

molecule is 22.7% larger than that of H_2O (in excellent agreement with the experimental value [33] of 23.1%).

(ii) The proton affinity of $(H_2O)_2$ is 19% larger than for the H_2O monomer, and that of $(NH_3)_2$ 12% larger than that of NH_3 (see Δ_1 in Table 1).

(iii) The proton affinity of $(NH_3)_2$ is larger than that of $(H_2O)_2$ (by 16.7%) and the value for $(NH_3)(H_2O)$ is intermediate between the two (larger by $\approx 11\%$ than that of $(H_2O)_2$).

Comparison of the solvation energies (Δ_2 in Table 1) shows that:

(i) The hydration energy of the hydronium ion (i.e. the binding energy of H_2O to H_3O^+) is 25% larger than the binding energy of NH_3 to NH_4^+.

(ii) The hydration energy of H_3O^+ is 76% larger than that of NH_4^+, and the dissociation energy of $(NH_3)(H_2O)H^+$ into $H_3O^+ + NH_3$ is about three

---

[1] In the mixed $(H_2O)(NH_3)H^+$ molecular ion (not shown in Fig. 1) the proton bond is nearly linear (i.e. $\angle(NH^+ O) = 177.9°$) with $d_{OH^+} = 1.56$ Å, and $d_{NH^+} = 1.07$ Å (reflecting the higher proton affinity of the ammonia molecule). The bonding proton lies on the symmetry axis of each of the bonded molecules. The plane of the water molecule is normal to the $NH^+ O$ plane, and one of the NH bonds of the ammonia molecule is in the $NH^+ O$ plane.

times larger than that for dissociation into NH_4^+ + H_2O. Comparing the results for $(NH_3)_2H^+$ and $(NH_3)(H_2O)H^+$ we note that the solvation energy by NH_3 is 2.2 times larger for H_3O^+ than for NH_4^+.

4. All-quantum dynamics of H_3O^+ and $H_5O_2^+$ clusters

We turn next to a discussion of results, illustrating application of the AQMD method, for H_3O^+ and $(H_2O)_2H^+$ at 150 K. In these simulations the electronic structure was calculated within LDA (i.e. without exchange–correlation gradient corrections; a plane-wave energy cutoff $E_c = 96$ Ry was used in the simulations). First we show in Fig. 2a for H_3O^+ the distribution of distances of the protons from the oxygen, obtained via the AQMD method (solid line), and compare it with the results obtained via BO-LDA-MD simulations (dashed line, where the protons were treated classically) at the same temperature. As seen from Fig. 2a the OH distances are distributed over a broader range when the protons are treated quantum mechanically. The average value at 150 K for d_{OH} in H_3O^+ calculated from the BO-LDA-MD simulations (that is with the protons treated classically) is $\bar{d}_{OH} = 1.852\,a_0$ (in this part we use the Bohr radius $a_0 = 0.52918$ Å as the unit of length), and the expectation value from the AQMD simulation is $\langle d_{OH} \rangle = 1.866\ a_0$ compared to a value of 1.844 a_0 calculated with no xcg corrections for the optimal (zero temperature) structure of H_3O^+.

For $(H_2O)_2H^+$, the distance distributions for d_{OH} in the H_2O molecules and for the distance d_{OH^+} between the oxygens and the 'intermolecular' proton, obtained from the BO-LDA-MD (dashed) and AQMD (solid line) simulations, are shown in Fig. 2b. Again the distance distributions obtained via the AQMD simulations are broader, and the d_{OH^+} distributions are broader than those for d_{OH}. The average values obtained via the BO-LDA-MD method are $\bar{d}_{OH} = 1.833\ a_0$ and $\bar{d}_{OH^+} = 2.256\ a_0$, and the expectation values from the AQMD simulation are $\langle d_{OH} \rangle = 1.849\ a_0$ and $\langle d_{OH^+} \rangle = 2.281\ a_0$, compared to $d_{OH} = 1.827\ a_0$ and $d_{OH^+} = 2.242\ a_0$ in the optimal (zero temperature) LDA (with no xcg) structure.

Further characterization of the intermolecular proton in $(H_2O)_2H^+$ is given in Fig. 3, where we show
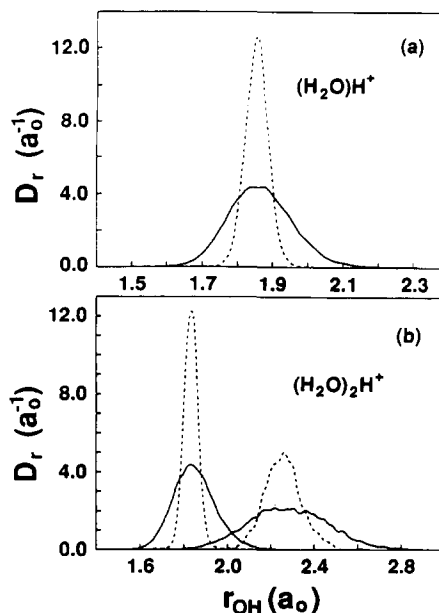
Fig. 2. Normalized distributions of distances between the protons and the oxygen in (a) $(H_2O)H^+$ and (b) $(H_2O)_2H^+$. Results are shown for simulations at 150 K where the protons were treated classically (BO-LDA-MD, denoted by dashed lines) and for AQMD simulations where the protons were treated quantum mechanically (solid lines). In (b) the distributions peaked about $\approx 1.8\ a_0$ correspond to the OH distance in the water molecules and those peaked about 2.2 a_0 correspond to the distance between the intermolecular proton and the molecular oxygens. Distance in units of the Bohr radius $a_0 = 0.52918$ Å.

the distributions (obtained via BO-LDA-MD and AQMD simulations) of the magnitude of the projection of the position vector of the proton on the normal plane bisecting the interoxygen vector (D_ρ in Fig. 3a), the distribution of the projection on the interoxygen vector (D_z in Fig. 3b), and the distribution of the magnitude of the distance between the proton and the midpoint of the interoxygen distance (D_r in Fig. 3c). We observe that the effect of the quantum treatment of the proton is to broaden these distributions, and that the width of the distributions reflects a rather shallow potential energy surface for motion of the 'bonding' proton. Further analysis of the dihedral angle distribution and that of the angle between the two H_2O molecular planes indicates that $(H_2O)_2H^+$ is a rather 'floppy' molecular ion, with low-frequency librations of the H_2O molecules. Another interesting finite-temperature feature of the

$(H_2O)_2H^+$ molecular ion revealed by the simulations is exhibited in Fig. 3d where the calculated distributions of the difference between the distances of the intermolecular proton from the two oxygens of
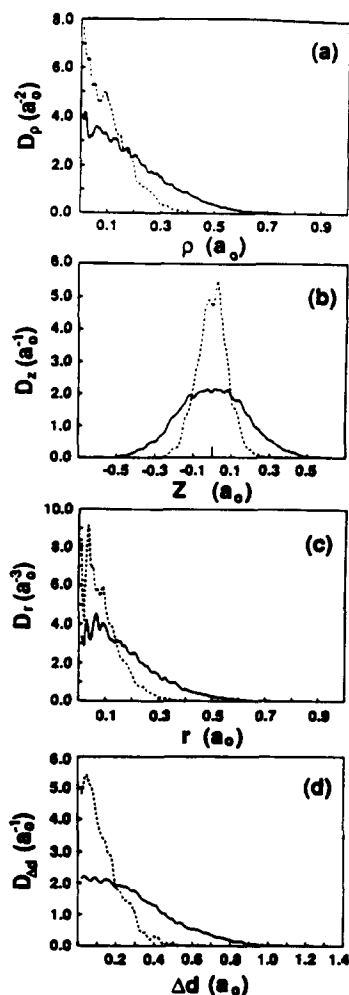
Fig. 3. (a)–(c) Distributions of the projections of the vector position of the intermolecular proton in $(H_2O)_2H^+$ on the normal plane bisecting the interoxygen vector (D_ρ, in (a)), and on the interoxygen vector (D_z, in (b)). Distributions of the distance between the intermolecular proton and the midpoint of the interoxygen vector are shown in (c). Shown in (d) are distributions of the difference between the distances of the intermolecular proton and the two molecular oxygens, $\Delta d = |d_{O_1H^+} - d_{O_2H^+}|$. Results obtained via AQMD simulations are given by solid lines, and those obtained from BO-LDA-MD simulations are given by dashed lines. Both simulations were performed at 150 K. Distances are given in units of a_0.

the water molecules are shown. We note that values of the difference $\Delta d = |d_{O_1H^+} - d_{O_2H^+}|$ (where O_1 and O_2 are the oxygens of the proton-bonded water molecules) obtained in the AQMD simulations (at 150 K) can achieve values which are up to twice those obtained in BO-LDA-MD simulations where the protons are treated classically (dashed line). Moreover we observed some correlation between Δd and the magnitude of the interoxygen distance, indicating that larger values of Δd correspond to larger intermolecular distances (i.e. larger interoxygen separations). We expect that at higher temperature one may observe even larger variations in Δd, correlated with larger values of the interoxygen distance, resulting in the occurrence of configurations of ionic character $(H_3O^+ \cdot H_2O$ and $H_2O \cdot H_3O^+)$ in the equilibrium ensemble (in this context we note that for a certain interoxygen distance the transfer of a proton from H_3O^+ to H_2O involves a potential barrier, which collapses for smaller intermolecular distances).

Further characteristics of the quantum nature of the protons in H_3O^+ and $(H_2O)_2H^+$ are provided by

$$R_T = \frac{P}{P-1}\left(\sum_{i=1}^{P} \langle (r_i - r_{i+1})^2 \rangle \right)^{1/2}, \qquad (12)$$

where r_i is the position of the ith bead (pseudo-particle) on the isomorphic necklace (see Section 2), and the imaginary time correlation function [10]

$$\mathscr{R}^2(t-t') = \langle |r(t) - r(t')|^2 \rangle,$$

$$0 \leqslant t - t' \leqslant \beta\hbar. \qquad (13)$$

The above quantities, which can be calculated for each of the protons, reduce for a free particle to $R_T^f = \sqrt{3}\,\lambda$ where λ is the thermal wave length $(R_T^f(150$ K, $H^+) = 1.855\ a_0)$, and $\mathscr{R}_f^2(t-t') = 3\lambda^2(t-t')(\beta\hbar - t + t')/(\beta\hbar)^2$, which for $t - t' = \frac{1}{2}\beta\hbar$ (diameter of the necklace) takes the value $\mathscr{R}_f^2(\frac{1}{2}\beta\hbar) = \frac{3}{4}\lambda^2$ $(\mathscr{R}_f((\frac{1}{2}\beta\hbar); 150$ K, $H^+) = 0.927\ a_0)$.

The value for R_T (averaged over the three protons) for H_3O^+ obtained in our simulations is 1.588 a_0; R_T for the molecular hydrogens in $(H_2O)_2H^+$ was obtained as 1.523 a_0, while the value for the intermolecular proton is 1.243 a_0, all of which are smaller than R_T^f at 150 K.
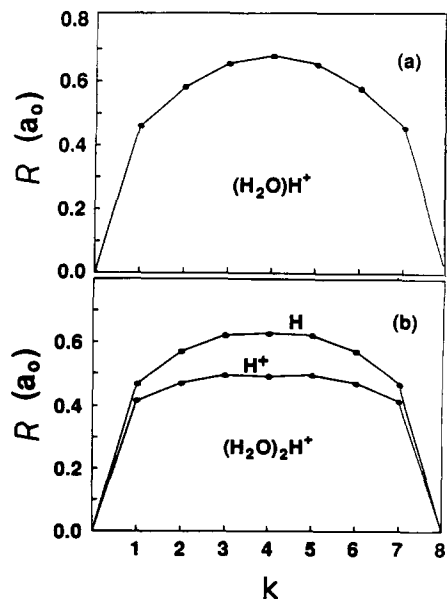
Fig. 4. Imaginary time correlation functions $\mathscr{R}$, plotted versus k (where $0 \leqslant k(\beta\hbar/P) \leqslant \beta\hbar$), for the protons in H_3O^+ (in (a)) and for the molecular hydrogens and intermolecular proton in $(H_2O)_2H^+$ (in (b)). The results were obtained from AQMD simulations at 150 K, $\mathscr{R}$ is in units of a_0.

The imaginary time correlation functions $\mathscr{R}(t - t')$ for H_3O^+ and $(H_2O)_2H^+$ are shown in Figs. 4a and 4b, respectively (in the Fig. 4b we display $\mathscr{R}$ for both the molecular hydrogens, and for the intermolecular proton). First we observe that for both the protonated clusters $\mathscr{R}(\frac{1}{2}\beta\hbar)$ is smaller than its value for a free proton at 150 K. We also note that the character of the variation of $\mathscr{R}$ with k (where k is an index of the pseudo-particle on the classical isomorphic closed necklace, i.e. $0 \leqslant t - t' = k(\beta\hbar/P) \leqslant \hbar\beta$) is different for H_3O^+ and for $(H_2O)_2H^+$ (see in particular Fig. 4b for H^+). Thus while for H_3O^+ $\mathscr{R}$ varies in a manner similar to that predicted for a free particle (see expression for $\mathscr{R}_f(t - t')$ following Eq. (13)), those for $(H_2O)_2H^+$ (and in particular the one corresponding to the intermolecular proton) exhibit a region in $t - t'$ where $\mathscr{R}$ saturates. This characteristic behavior is termed ground-state dominance [8], occurring when $\beta\Delta E \gg 1$, where ΔE is the energy gap between the ground-state and the first excited state of the particle. From the above we conclude that while for the protons in H_3O^+ and (to a somewhat lesser extent) the molecu-

lar hydrogens in $(H_2O)_2H^+$, low-lying excitations of the quantized nuclear reactions are populated at 150 K, the ground-state dominates for the intermolecular proton in $(H_2O)_2H^+$.

The structure and the nature of the inversion tunneling in the hydronium ion, H_3O^+, have been the subject of a number of experimental and theoretical studies [24–26]. The structure of H_3O^+ has a pyramidal geometry [2], similar to its isoelectronic counterpart NH_3. Our generalized gradient correction (GGC) LDA calculations with a plane wave cutoff $E_c = 158$ Ry (a 54^3 grid, with a grid spacing of 0.25 a_0) yield an inversion barrier of 0.064 eV (516 cm^{-1}) compared to a barrier of 672 cm^{-1} obtained via analysis of high-resolution spectroscopic measurements [25,26] (in LDA calculations with no xcg corrections and with a lower plane-wave energy cutoff $E_c = 96$ Ry, a lower barrier of 0.033 eV was obtained).

While a determination of the inversion rate using the path-integral based AQMD simulations is feasible using the 'centroid method' [9], we show in Fig. 5 (top) results for the distribution of $u = \cos\theta$ (θ is the angle subtended between the vector normal to the hydrogen plane to the oxygen and an OH bond vector) obtained at 150 K via BO-LDA-MD simulations (with classical protons, dashed line) and AQMD simulations (with the protons treated quantum mechanically via the PI method, solid line). As noted before, in these simulations the electronic Born–Oppenheimer potential surfaces were calculated using LDA, with no xcg correction, with $E_c = 96$ Ry; the corresponding calculated inversion barrier is 0.033

---

[2] In the optimal pyramidal geometry of H_3O^+ the calculated ($E_c = 96$ Ry with GGC) OH distance is $d_{OH} = 1.859$ a_0 (1.851 a_0 for $E_c = 158$ Ry) with an angle $\angle(HOH) = 114.2°$; the height of the oxygen above the three hydrogen plane is $h_0 = 0.461$ a_0 (0.452 a_0 for $E_c = 158$ Ry) and the angle between the normal to the hydrogen plane to the oxygen and an OH bond is $\theta = 75.85°$ (the $\angle(HOH)$ and θ angles are the same for both $E_c = 96$ and 158 Ry calculations). In the transition state for inversion the geometry of H_3O^+ is of course planar with $d_{OH} = 1.849$ a_0 (1.837 a_0 for $E_c = 158$ Ry) and $\angle(HOH) = 120°$ (in calculations with $E_c = 96$ Ry and no xcg corrections $d_{OH} = 1.849$ a_0, and $h_0 = 0.417$ a_0, $\angle(HOH) = 115°$ and $\theta = 76.95°$ for the pyramidal geometry, and $d_{OH} = 1.849$ a_0 for the planar transition-state configuration). These values are in agreement with those used in the analysis of spectroscopical data for H_3O^+ [26,27].
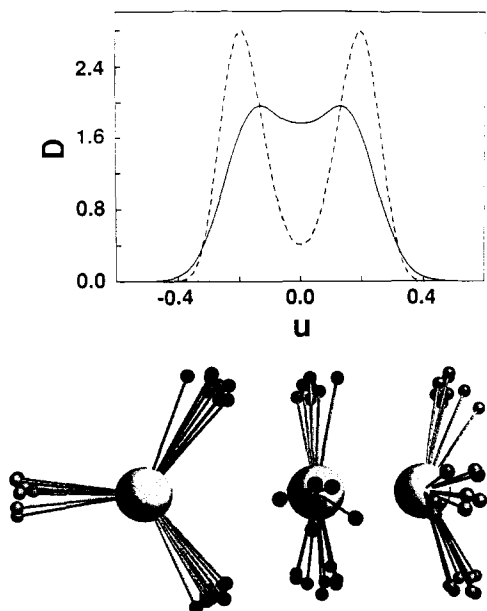
Fig. 5. Top: distributions of $u = \cos\theta$, where θ is the angle in H_3O^+ between an OH bond and the vector normal to the plane of the hydrogens to the oxygen atom. Results obtained from simulations at 150 K, using the BO-LDA-MD method (classical protons; dashed line) and the AQMD method (quantum protons, solid line), are shown. $u = 0$ corresponds to the inversion planar transition-state configuration. Note the quantum enhancement of the inversion probability indicated by an increase in the probability to find the system in the vicinity of the transition state. (Bottom) Snap shots of configurations taken from AQMD simulations of H_3O^+ at 150 K. The large sphere corresponds to the oxygen atom and the small spheres represent the pseudo-particles of the classical isomorphim ($P = 8$ pseudo-particles representing each proton). The configuration on the right corresponds to a pyramidal structure of H_3O^+, and the ones at the middle (side view) and left (top view) show a representative transition-state structure.

eV (i.e. 373 K), which is over twice the temperature of the simulations (150 K). A value of $u = 0$, in Fig. 5, corresponds to the inversion saddle (transition state) planar configuration (see a snapshot, taken from the AQMD simulation, shown at the bottom of Fig. 5) and other values of u (positive and negative on the two sides of the saddle) correspond to pyramidal configurations, see e.g., right configuration at the bottom of Fig. 5 (i.e. a change of sign of u corresponds to an inversion). Comparison between the results obtained via the two simulations provides a measure of the quantum enhancement of the inversion process. Further simulations (including GGC) to determine the inversion rate are in progress.

5. Summary

We have presented a novel method which unifies the quantum path-integral description of the ionic degrees of freedom with the BO-LDA-MD methodology [4], thus allowing investigations of physical systems where both the electronic and nuclear degrees of freedom are treated quantum mechanically (the all-quantum MD simulation method, AQMD, described in Section 2).

Our simulations of H_3O^+ and $(H_2O)_2H^+$ at 150 K demonstrate broadening of the distributions of internuclear distances involving the hydrogens due to their quantum nature. In the proton-bonded $(H_2O)_2H^+$, which may be written also as $(H_2O)H^+(H_2O)$, the state of the intermolecular proton is characterized by ground-state dominance (see Fig. 4) and our results for the spatial distribution of the proton suggest that at higher temperatures configurations of ionic character (i.e. $H_3O^+ \cdot H_2O$ and $H_2O \cdot H_3O^+$) may develop. Finally, a measure of the quantum enhancement of the inversion isomerization in H_3O^+, at 150 K, was demonstrated.

Acknowledgement

References

[1] G. Ciccotti, D. Frenkel and I.R. McDonald, eds., Simulations of liquids and solids (North-Holland, Amsterdam, 1987).
[2] R.N. Barnett, U. Landman, G. Rajagopal and A. Nitzan, Israel J. Chem. 30 (1990) 85.
[3] R. Car and M. Parrinello, Phys. Rev. Letters 55 (1985) 2471.
[4] R.N. Barnett and U. Landman, Phys. Rev. B 48 (1993) 2081.
[5] G. Galli and M. Parrinello, in: Computer simulations in materials science, eds. M. Meyer and V. Pontikis (Kluwer, Dordrecht, 1991) p. 283.

[6] U. Landman, R.N. Barnett, H.-P. Cheng, C.L. Cleveland and W.D. Luedtke, in: Computations for the nano-scale, eds. P.E. Blochl, C. Joachim and A.J. Fisher (Kluwer, Dordrecht, 1993) p. 75.

[7] R.P. Feynman and A.R. Hibbs, Quantum mechanics and path integrals (McGraw-Hill, New York, 1965).

[8] D. Chandler, in: Liquids, freezing and glass transition, eds. J.P. Hansen, D. Levesque and J. Zinn-Justin (Elsevier, Amsterdam, 1991);
D. Chandler and K. Leung, Annu. Rev. Phys. Chem. 45 (1994).

[9] M.J. Gillan in Computer Modeling of Fluids, Polymers and Solids, eds. C.R.A. Catlow et al. (Kluwer, Dordrecht, 1990), p. 155.

[10] B.J. Berne and D. Thirumali, Ann. Rev. Phys. Chem. 37 (1986) 401.

[11] U. Landman, R.N. Barnett, J. Luo, D. Scharf and J. Jortner, in: Few-body systems and multiparticle dynamics, ed. D.A. Micha, AIP Conf. Proc. No. 162 (AIP, New York, 1987) p. 200.

[12] P.J. Rossky and J. Schnitker, J. Phys. Chem. 92 (1988) 4277.

[13] R.P. Feynman, Phys. Rev. 56 (1939) 340.

[14] N. Troullier and J.L. Martins, Phys. Rev. B 43 (1991) 1993.

[15] S.H. Vosko, L. Wilks and M. Nusair, Can. J. Phys. 58 (1980) 1200;
S.H. Vosko and L. Wilks, J. Phys. C 15 (1982) 2139.

[16] A.D. Becke, Phys. Rev. A 38 (1988) 3098; J. Chem. Phys. 96 (1992) 2155.

[17] J.P. Perdew, Phys. Rev. B 33 (1986) 8822; 34 (1986) 7046.

[18] M. Parrinello and A. Rahman, J. Chem. Phys. 80 (1984) 860.

[19] U. Landman, R.N. Barnett, C.L. Cleveland and P. Norlander, in: Tunneling, eds. J. Jortner and B. Pullman (Reidel, Dordrecht, 1986), p. 269.

[20] T.R. Mattson, U. Engberg and G. Wahnstrom, Phys. Rev. Letters 71 (1993) 2615.

[21] A. Kuki and P.G. Wolynes, Science 236 (1987) 1647.

[22] D.M. Ceperley and E.L. Pollock, Phys. Rev. Letters 56 (1986) 351;
P. Sindzingre, M. L. Klein and D.M. Ceperley, Phys. Rev. Letters 63 (1989) 1601.

[23] C.L. Cleveland, U. Landman and R.N. Barnett, Phys. Rev. B 39 (1989) 117.

[24] R.J. Saykally, Science 239 (1988) 157;
J.V. Coe and R.J. Saykally, in: Ion and cluster ion spectroscopy and structure, ed. J.P. Maier (Elsevier, Amsterdam, 1989) p. 131;
C.S. Guteman and R.J. Saykally, Ann. Res. Phys. Chem. 35 (1984) 387.

[25] T.J. Sears, P.R. Bunker, P.B. Davies, S.A. Johnson and V. Spirko, J. Chem. Phys. 83 (1985) 2676.

[26] D.-J. Liu, T. Oka and T.J. Sears, J. Chem. Phys. 84 (1986) 1312.

[27] Y.I. Yeh, Y.T. Lee and J.T. Hougen, J. Mol. Spectry. 164 (1994) 473, and references therein.

[28] Z. Shi, J.V. Ford, S. Wei and A.W. Castleman Jr., J. Chem. Phys. 99 (1993) 8009.

[29] M.J. Frisch, J.E. Del Bene, J.S. Binkley and H.F. Schaefer III, J. Chem. Phys. 84 (1986) 2279.

[30] E.P.F. Lee and J.M. Dyke, Mol. Phys. 73 (1991) 375, and references to earlier studies therein.

[31] Y. Xie, R.B. Remington and H.F. Schaefer III, J. Chem. Phys. 101 (1994) 4878, and references therein.

[32] R.N. Barnett, H.-P. Cheng, H. Hakkinen and U. Landman, J. Phys. Chem., in press.

[33] P.L. Huyskens, W.A.P. Luck, and T. Zeegers-Huyskens, eds. Intermolecular forces (Springer, Berlin, 1991);
E. Caldin and V. Gold, eds. (Chapman and Hall, London, 1975).

[34] A.J. Cunningham, J.D. Payzant and P. Kebarle, J. Am. Chem. Soc. 94 (1972) 7627.

[35] R.G. Keesee and A.W. Castleman Jr., J. Phys. Chem. Ref. Data 15 (1986) 1011.